

# Vacuum polarization alters the spectra of accreting X-ray pulsars

E. Sokolova-Lapa<sup>1\*</sup>, J. Stierhof<sup>1</sup>, T. Dauser<sup>1</sup>, and J. Wilms<sup>1</sup>

Dr. Karl Remeis-Observatory and Erlangen Centre for Astroparticle Physics, Friedrich-Alexander Universität Erlangen-Nürnberg, Sternwartstr. 7, 96049 Bamberg, Germany

Received ... / Accepted ...

## ABSTRACT

It is a common belief that for magnetic fields typical for accreting neutron stars in High-Mass X-ray Binaries vacuum polarization only affects the propagation of polarized emission in the neutron star magnetosphere. We show that vacuum resonances can significantly alter the emission from the poles of accreting neutron stars. The effect is similar to vacuum polarization in the atmospheres of isolated neutron stars and can result in suppression of the continuum and the cyclotron lines. It is enhanced by magnetic Comptonization in the hot plasma and proximity to the electron cyclotron resonance. We present several models to illustrate the vacuum polarization effect for various optically thick media and discuss how the choice of polarization modes affects the properties of the emergent radiation by simulating polarized energy- and angle-dependent radiative transfer. Polarization effects, including vacuum polarization, crucially alter the emission properties. Together with strongly angle- and energy-dependent magnetic Comptonization, they result in a complex spectral shape, which can be described by dips and humps on top of a power-law-like continuum with high-energy cutoff. These effects provide a possible explanation for the common necessity of additional broad Gaussian components and two-component Comptonization models that are used to describe spectra of accreting X-ray pulsars. We also demonstrate the character of depolarization introduced by the radiation field's propagation inside the inhomogeneous emission region.

**Key words.** X-rays: binaries – stars: neutron – methods: numerical – radiative transfer - polarization - magnetic fields

## 1. Introduction

The formation of the X-ray spectra of accreting highly magnetized ( $B \sim 10^{12}$  G) neutron stars in High-Mass X-ray Binaries (HMXBs) is a complex process. The emitted continuum is mainly shaped by magnetic Comptonization in an accretion column or accretion mound. Resonant Compton scattering also results in the appearance of absorption line-like features in the spectra, or “cyclotron lines” (Staubert et al. 2019). Recent observations have revealed the complexity of continuum shapes, which often cannot be described only by a simple power law with high-energy cutoff (Müller et al. 2013), but require additional broad Gaussian features in absorption or emission at intermediate energies (also known as the “10-keV” feature; see, e.g., Ferrigno et al. 2009; Diez et al. 2022). Alternatively, the continuum can be described as the sum of two Comptonization spectra from plasmas with different temperatures (see, e.g., Doroshenko et al. 2020). In contrast, the available angle- and polarization-averaged models for continuum formation (e.g., Becker & Wolff 2007; West et al. 2017a,b) yield a smooth spectral shape. The rich observational background therefore remains ahead of the spectral modeling, calling for new emission models that incorporate further physics, such as the effects of polarization and angular redistribution.

Polarization of radiation in the strong magnetic field introduces further complexity in the modeling. Apart from the magnetoactive plasma, photon polarization states can be affected by the quantum electrodynamic (QED) effect known as vacuum polarization. For the cold, absorption-dominated inhomogeneous atmospheres of highly magnetized isolated neutron stars ( $B \sim 10^{14}$  G), radiative transfer solutions were obtained (e.g.,

Lai & Ho 2002; Ho & Lai 2003; Özel 2003), some of which also included partial mode conversion (Ho & Lai 2004; van Adelsberg & Lai 2006). For the lower fields characteristic of accreting neutron stars in HMXBs, however, the vacuum resonance has not been included in the radiative transfer discussions of the last three decades. Early studies of vacuum polarization effects by Pavlov & Shibano (1979), Ventura et al. (1979), Kaminker et al. (1982), and Soffel et al. (1985) addressed the importance of this phenomenon for homogeneous media only, without Compton scattering, finding that in this case the vacuum resonance results in a narrow low-energy absorption feature. Meszaros & Nagel (1985a,b) noted the importance of the combined vacuum and plasma polarization modes for the shape of the cyclotron line profile based on their homogeneous models including Comptonization, but no qualitative comparison with other cases was made. Later models for the accretion column and atmospheric emission considered only the polarization-averaged case (see, e.g., Becker & Wolff 2007; Farinelli et al. 2016; West et al. 2017b) or used pure magnetized plasma (Mushtukov et al. 2021; Caiazzo & Heyl 2021a,b) and pure vacuum normal modes (Sokolova-Lapa et al. 2021). Models for cyclotron lines on top of a predefined continuum also largely focused on the pure vacuum case (see, e.g., Araya & Harding 1999; Schwarm et al. 2017a,b).

Previous claims that for  $B \sim 10^{12}$  G vacuum polarization does not alter the emission spectra (Ho & Lai 2004; van Adelsberg & Lai 2006) should be taken with a grain of salt, as they were based on computations for cool absorption-dominated atmospheres. Vacuum polarization in the hot Comptonizing medium of accreting highly-magnetized neutron stars thus remains poorly studied. Here, we would like to highlight the effect of vacuum polarization in these environments and demonstrate its possible influence on the spectral shape and polarization sig-

\* e-mail: ekaterina.sokolova-lapa@fau.de

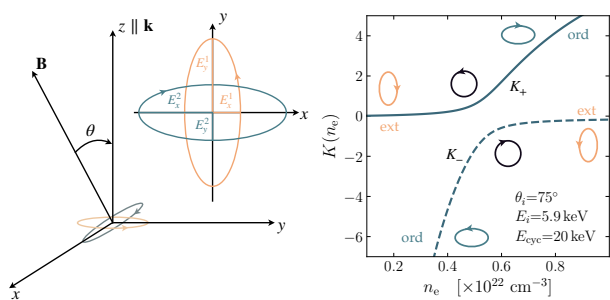


**Fig. 1.** *Left:* Coordinate system chosen to define ellipses of the polarization modes. *Right:* Dependency of the ellipticity of the polarization modes on the electron number density. The vacuum resonance occurs in the center of the figure. Based on Fig. 1 from Lai & Ho (2003).

nal. We perform a comparison for different choices of photon normal modes. We introduce the problem of the mode definition in Sect. 2. In Sect. 3, we present several models for emission from homogeneous and inhomogeneous media. Section 4 provides the discussion and conclusion of this study.

## 2. Polarization modes

The highly magnetized plasma in the vicinity of a neutron star is a complex medium, which can support various types of waves. In the medium, transverse electromagnetic waves, with electric vector,  $\mathbf{E}$ , perpendicular to the wave vector,  $\mathbf{k}$ , are allowed to propagate at frequencies higher than the electron plasma frequency. For modeling the X-ray emission from accreting neutron stars in HMXBs, the description of the radiation field in terms of two transverse waves, the two polarization normal modes, became a standard approach. We outline the classical definition of the two modes in Sect. 2.1 and discuss their ambiguity when both, the plasma and the QED vacuum alter the radiation propagation in Sect. 2.2.

### 2.1. Mode definition and ellipticity

For high-energy radiation in a magnetoactive plasma with  $B \sim 10^{12}$  G, the electron response governs wave propagation. The solution of the wave equation with a linear response in the form of two independent modes is known for different temperature regimes (e.g., Ventura 1979; Pavlov et al. 1980; Nagel 1981). The polarization vectors,  $\mathbf{E}$ , of the two normal modes have opposite directions of rotation. The modes are elliptically polarized, where the ellipticity  $K = E_x/E_y$  in a coordinate system in which the  $z$ -axis is parallel to  $\mathbf{k}$  (Fig. 1, left). The “ordinary” mode is defined as the left-hand polarized wave, with  $\mathbf{E}$  oscillating mainly in the  $(\mathbf{B}, \mathbf{k})$ -plane ( $|K| \gg 1$ ), where  $\mathbf{B}$  is the external magnetic field vector. The polarization vector of the right-hand polarized “extraordinary” mode oscillates mainly perpendicularly to this plane ( $|K| \ll 1$ ). For the extraordinary mode, the co-directional rotation of  $\mathbf{E}$  with electrons in the external  $B$ -field allows the mode to resonate at the cyclotron frequency. In the absence of damping, the ellipses of the two modes are of equal shape, perpendicular to each other.

The effect of vacuum polarization in a strong  $B$ -field alters this picture due to the birefringence introduced by QED’s virtual electron-positron plasma, which allows both modes to exhibit cyclotron resonances. In the absence of a real plasma, the equality of the virtual charges makes the normal modes linear and strictly orthogonal to each other (except for  $\mathbf{k} \parallel \mathbf{B}$ ). The combined effect of the virtual and the real plasma results in a more

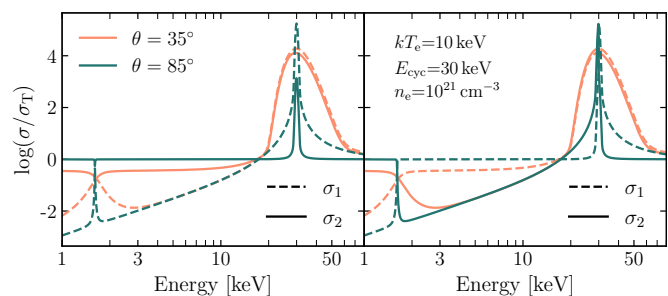


**Fig. 2.** Cross sections for magnetic Compton scattering for two different propagation angles,  $\theta$ . The modes are shown *left*: for the case of discontinuous and *right*: continuous refractive indices for  $B \approx 2.6 \times 10^{12}$  G.

complex behavior of the modes, causing occasional departure from orthogonality.

### 2.2. Mode ambiguity

For a given  $B$ -field, a given electron number density of the plasma,  $n_e$ , and a photon propagation angle,  $\theta$ , there are certain photon energies at which the effects of real and virtual particles compensate each other, since the QED vacuum and the plasma enforce linear polarization of the modes in a mutually orthogonal direction (Lai & Ho 2003). The two most relevant of these are at the vacuum resonance,  $E_V$ , which depends on  $n_e$  and  $B$  (see, e.g., Ho & Lai 2003), and the cyclotron resonance,  $E_{\text{cyc}}$ . The transition through these points results in a flip of the position angle of the polarization ellipse by  $\pm 90^\circ$  or in the reversal of the direction of the rotation of the polarization vector due to the switch in the dominance of the influence of vacuum and plasma (Pavlov & Shibano 1979). These effects make the classical definition of the modes introduced in Sect. 2.1 internally inconsistent. As discussed by Kirk (1980), a general definition of the modes can be made based on the continuity of the refractive indices of the waves. Figure 2 shows the cross section for magnetic Compton scattering as a function of photon energy, illustrating the effect of the continuity of the refractive index across the spectrum. In the case of a discontinuous refractive index, corresponding to the change of the wave’s handedness, the cross sections of the modes acquire a sharp, resonance-like feature at  $E_V$  (Ventura et al. 1979). The alternative choice of continuous refractive indices results in an abrupt change of opacity (see, e.g., Meszaros & Nagel 1985a).

The problem of the mode definition becomes clear when one considers the propagation in an inhomogeneous medium, where a photon passes, e.g., from a plasma-dominated region where its energy  $E > E_V$ , to a vacuum-dominated one, where  $E < E_V$ . After passing the “resonant density” where  $E = E_V$ , modes with  $|K| \ll 1$  and  $|K| \gg 1$  will acquire left-hand and right-hand polarization, respectively. Figure 1 (right) illustrates the behavior of the modes’ ellipticity in an inhomogeneous medium. For a smooth density gradient, at energies above a few keV it is expected that the modes evolve adiabatically (i.e., they keep their original helicity), while they behave non-adiabatically at lower energies (Özel 2003; Ho & Lai 2003). In general, however, the probability of a jump of mode characteristics across the resonance has to be considered (van Adelsberg & Lai 2006). The adiabatic and non-adiabatic cases correspond to the continuous and discontinuous behavior of the refractive index, respectively. In the following, we use the notations “mode 1” and “mode 2” as denoted for these cases in Fig. 2 by  $\sigma_{1,2}$ .

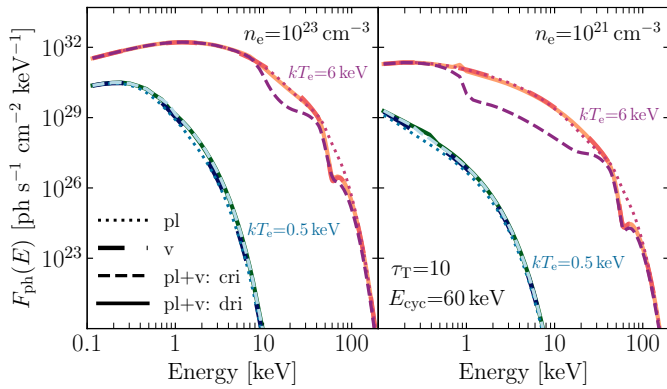


**Fig. 3.** Flux from a homogeneous slab summed over the two polarization modes for the higher (left) and lower (right) electron number density, for  $B \approx 5.2 \times 10^{12}$  G. Different types of polarization modes are shown: pure plasma (“pl”, dotted), pure vacuum (“v”, thick dashes), modes and modes with continuous/discontinuous (“pl+v: cri/dri”, dashed/solid) refractive indices.

### 3. Modeling and Results

We use our polarization-dependent radiative transfer code FINRAD, which takes into account angular and energy redistribution of photons both in the continuum and in the cyclotron line to investigate the effect of vacuum polarization. The code is based on the Feautrier numerical scheme for two polarization modes (Nagel 1981; Meszaros & Nagel 1985a). More details on the implementation and verification of the code are given by Sokolova-Lapa et al. (2021). We perform each simulation for both choices of the cross section behavior displayed in Fig. 2. For the inhomogeneous model, this choice corresponds to the adiabatic and non-adiabatic mode propagation. For some models we present a comparison with the modes for pure plasma (hot, but non-relativistic) and pure vacuum. All models assume a slab-like emission region, with the  $\mathbf{B}$ -field parallel to the surface normal (same as in Nagel 1981). The slab is characterized by  $n_e$ , the constant  $\mathbf{B}$ -field value, and the electron temperature  $kT_e$ . The treatment for induced processes and boundary conditions are the same as in Sokolova-Lapa et al. (2021), i.e., diffusion limit at the bottom of the slab and no illumination from the top. We describe the spectral shape with the photon flux  $F_{\text{ph}}(E) = 4\pi \int_0^1 I(E, \theta) \cos(\theta)/E d\theta$ , where the specific intensity  $I(E, \theta)$  is obtained with FINRAD. The angular dependence of the emission will be discussed in future studies. Section 3.1 presents the spectra from several homogeneous models for various  $kT_e$ ,  $n_e$ , and  $B$ . In Sect. 3.2, we then construct a simple model for an accretion mound with an inhomogeneous density profile and show the resulting spectra and polarization signal.

#### 3.1. Homogeneous slab

Figure 3 illustrates the influence of vacuum polarization on the total spectra of the emission from the homogeneous slab, and compares the spectra obtained for the pure plasma and the vacuum cases. The choice of modes for the low-temperature case ( $kT_e = 0.5$  keV, spectra with lower flux) has a very minor effect on the spectral shape. The Comptonized spectra for the hotter plasma,  $kT_e = 6$  keV, illustrate the strong influence of the cyclotron resonance near the cyclotron energy  $E_{\text{cyc}} = 60$  keV for all cases except for the pure plasma spectra. The latter are dominated by mode 2 (in this case, the classically-defined ordinary

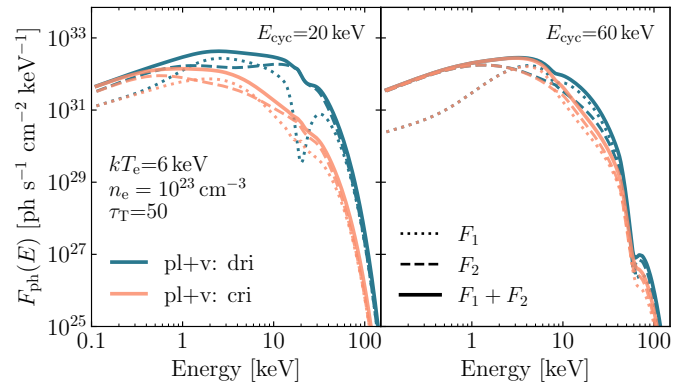


**Fig. 4.** Emission from a highly magnetized optically thick slab for continuous and discontinuous behavior of the refractive indices, for two  $B$ -field values, left:  $B \sim 1.7 \times 10^{12}$  G ( $E_{\text{cyc}} = 20$  keV and  $E_V \sim 24$  keV) and right:  $B \sim 5.2 \times 10^{12}$  G ( $E_{\text{cyc}} = 60$  keV and  $E_V \sim 8$  keV).

mode), whose weak resonance is introduced by the Doppler effect on the thermal electrons and then washed out by angle averaging. The spectra for the case of the discontinuous refractive indices closely follow the pure vacuum ones, except for a small region near the vacuum resonance (the polarization signal, however, is different, see Sect. 3.2). The spectral shape for the case of the continuous refractive indices differs significantly from the others. There is a noticeable depression of the continuum above the vacuum resonance energy – vacuum polarization effectively reduces the total optical depth of the emitting region. Lai & Ho (2002) noted similar behavior in their studies of photon propagation in magnetar-like fields with  $B \sim 10^{14}$  G. When the vacuum resonance is located closer to the cyclotron line, it can mimic an additional line-like feature. For the cases presented in Fig. 3,  $E_V < E_{\text{cyc}}$ . Figure 4 (left) illustrates the case when  $E_V > E_{\text{cyc}}$  and shows contributions of the two normal modes. Here, the cyclotron line is significantly suppressed. The case of the continuous refractive indices is the most interesting one, as none of the modes exhibit a strong cyclotron resonance. The case of a higher  $B$ -field shown in Fig. 4 (right) ( $E_V \ll E_{\text{cyc}}$ ) yields a more complex continuum shape.

#### 3.2. Inhomogeneous accretion mound

In an inhomogeneous medium, the radiation field encounters the vacuum resonance at a continuum of energies. To understand how this effect contributes to the total spectrum, we create a simplified model of an accretion mound confined to the polar cap of a neutron star. The mound is represented by a slab of magnetized isothermal plasma with  $kT_e = 5$  keV and  $E_{\text{cyc}} = 40$  keV, a height of 500 m and a radius of 300 m. We assume that the plasma is accreted at a mass-accretion rate  $\dot{M} = 10^{17}$  g s $^{-1}$  and that the accretion flow is mainly decelerated higher up, above the emission region. The velocity on the top of the mound is set to the 5% of the free-fall velocity near the surface,  $v_{\text{ff}}$ , and decreases linearly within the mound to  $10^{-3}v_{\text{ff}}$  at the bottom, such that the density distribution within the mound increases from  $\sim 10^{22}$  cm $^{-3}$  at the top to  $\sim 10^{24}$  cm $^{-3}$  at the bottom.

Figure 5 shows the total flux for the previously discussed types of polarization modes. Here, the adiabatic and non-adiabatic cases (left panel) are similar, both exhibiting an imprint of the vacuum resonance at  $\sim 6.5$  keV from the most tenuous top layer of the slab. For adiabatic propagation the total flux is slightly suppressed above  $E_V$ , with the cyclotron line core be-

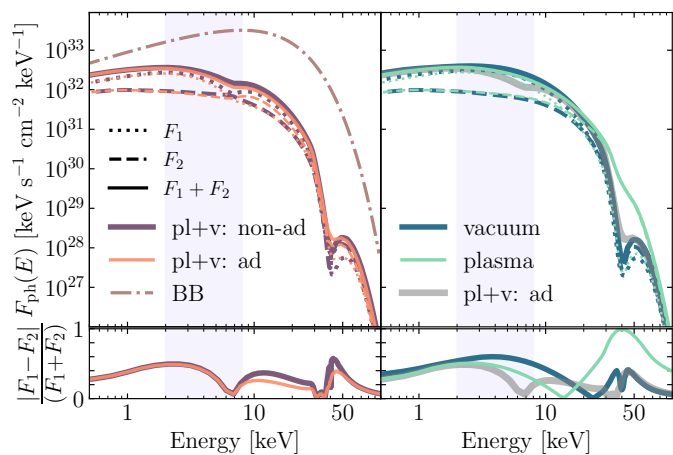


**Fig. 5.** *Top:* Flux from an inhomogeneous mound with  $kT_e = 5$  keV and  $B \sim 3.6 \times 10^{12}$  G ( $E_{\text{cyc}} = 40$  keV) for the cases including the plasma and vacuum polarization effects for non-adiabatic, “non-ad” and adiabatic, “ad”, mode propagation (*left*) and the pure plasma and vacuum cases (*right*). The left-top panel shows the corresponding blackbody spectrum (“BB”). *Bottom:* The corresponding degree of polarization. The energy range accessible by the Imaging X-ray Polarimetry Explorer (IXPE) is shown by the light-blue transparent region.

coming noticeably more shallow. Due to the absence of the vacuum resonance, the pure plasma and vacuum cases (right panel) naturally lack the additional complexity of the spectra.

For both cases, the polarization degree (Fig. 5, bottom) reaches a maximum of  $\sim 50\%$ <sup>1</sup>. It is overall lower than predicted by the accretion column model of [Caiazzo & Heyl \(2021b\)](#) for the emission in the neutron star rest frame. This difference is probably due to radiative propagation effects that were omitted by these authors, such as redistribution during scattering, which are enhanced by the presence of the hot plasma. The degree of polarization in the pure vacuum case is higher at intermediate energies; for the plasma case it reaches almost 100% near the cyclotron line.

#### 4. Discussion and Conclusions

In this work we presented the results of radiative transfer calculations in the hot Comptonizing medium in the vicinity of accreting neutron stars with  $B \sim 10^{12}$  G, including the effect of vacuum polarization. We found that the choice of polarization modes and the vacuum resonance can potentially strongly influence the emitted spectrum. Together with angle- and energy-dependent magnetic Comptonization, those polarization effects result in a complex continuum shape and can alter the cyclotron line. The natural switch in the dominance of the two polarization modes in the total flux across the spectrum produces excesses and dips on top of the power-law-like continuum. While this phenomenon is not specific for vacuum polarization, it is enhanced by it due to the additional interplay between the modes. The vacuum resonance itself can also introduce a weak dip in the spectra, mimicking the cyclotron line, as shown for the inhomogeneous model. For the conditions studied here, we find that pure vacuum normal modes provide a closer spectral shape to the mixed (magnetized plasma and polarized vacuum) case than pure plasma modes.

<sup>1</sup> For the angle-resolved spectra of our calculations, not presented here, the polarization degree reaches a maximum of  $\sim 65\%$  in the continuum, at  $\theta \sim 70^\circ$

The combination of these effects may also be able to explain several complexities observed in the spectra of accreting neutron stars in HMXBs, such as the “10-keV” feature, or the two-component-like continua. Stand-alone absorption line-like features at intermediate energies (see, e.g., [Reig & Milonaki 2016](#); [Doroshenko et al. 2020](#), for 4U 1901+03 and KS 1947+300) are potential candidates for the mode interchange regions. Vacuum polarization can also result in a significant suppression of the cyclotron line when  $E_V > E_{\text{cyc}}$ , potentially explaining the missing cyclotron lines in the spectra of some sources.

Concerning the polarization degree, our results for a simplified model of the accretion mound show a maximum at  $\sim 50\%$  in the continuum. The vacuum resonance results in a broad region of depolarization. A detailed understanding of the angular redistribution is important to draw any further conclusions, which will be addressed in the future work, along with the study of emission beaming and pulse profile formation under the influence of light bending. We expect that angle-dependent beaming and the propagation of the X-rays in the magnetosphere, will only lower the observable degree of polarization, bringing the total value closer to the low values observed recently by IXPE (see, e.g., [Tsygankov et al. 2022](#); [Doroshenko et al. 2022](#)). The presented model is a first step towards a more realistic description of the radiation field in the accretion channel, which ideally should include partial mode conversion, higher relativistic corrections, and consistent simulation of the structure of the accretion mound, as well as the influence of the falling flow.

*Acknowledgements.* This research has been funded by DFG grants WI1860/11-2 and WI1860/19-1. The work originates in part from the thesis draft by ESL. We are grateful to Aafia Zainab, Philipp Thalhammer, and Katrin Berger for their valuable comments. The authors also thank the XMAG collaboration and all participants of the workshop “X-ray Tracking of Magnetic Field Geometries in Accreting X-ray Pulsars”, who supported fascinating discussions and raised new inspiring questions for this research.

#### References

- Araya, R. A. & Harding, A. K. 1999, *ApJ*, 517, 334  
Becker, P. A. & Wolff, M. T. 2007, *ApJ*, 654, 435  
Caiazzo, I. & Heyl, J. 2021a, *MNRAS*, 501, 129  
Caiazzo, I. & Heyl, J. 2021b, *MNRAS*, 501, 109  
Diez, C. M., Grinberg, V., Fürst, F., et al. 2022, *A&A*, 660, A19  
Doroshenko, R., Piraino, S., Doroshenko, V., & Santangelo, A. 2020, *MNRAS*, 493, 3442  
Doroshenko, V., Poutanen, J., Tsygankov, S. S., et al. 2022, *Nature Astronomy*, 6, 1433  
Farinelli, R., Ferrigno, C., Bozzo, E., & Becker, P. A. 2016, *A&A*, 591, A29  
Ferrigno, C., Becker, P. A., Segreto, A., Mineo, T., & Santangelo, A. 2009, *A&A*, 498, 825  
Ho, W. C. G. & Lai, D. 2003, *MNRAS*, 338, 233  
Ho, W. C. G. & Lai, D. 2004, *ApJ*, 607, 420  
Kaminker, A. D., Pavlov, G. G., & Shibanov, I. A. 1982, *Ap&SS*, 86, 249  
Kirk, J. G. 1980, *Plasma Physics*, 22, 639  
Lai, D. & Ho, W. C. 2003, *Phys. Rev. Lett.*, 91, 071101  
Lai, D. & Ho, W. C. G. 2002, *ApJ*, 566, 373  
Meszaros, P. & Nagel, W. 1985a, *ApJ*, 298, 147  
Meszaros, P. & Nagel, W. 1985b, *ApJ*, 299, 138  
Müller, S., Ferrigno, C., Kühnel, M., et al. 2013, *A&A*, 551, A6  
Mushtukov, A. A., Suleimanov, V. F., Tsygankov, S. S., & Portegies Zwart, S. 2021, *MNRAS*, 503, 5193  
Nagel, W. 1981, *ApJ*, 251, 288  
Özel, F. 2003, *ApJ*, 583, 402  
Pavlov, G. G. & Shibanov, I. A. 1979, *Zh. Eksp. Teor. Fiz.*, 76, 1457  
Pavlov, G. G., Shibanov, I. A., & Iakovlev, D. G. 1980, *Ap&SS*, 73, 33  
Reig, P. & Milonaki, F. 2016, *A&A*, 594, A45  
Schwarm, F.-W., Ballhausen, R., Falkner, S., et al. 2017a, *A&A*, 601, A99  
Schwarm, F. W., Schönherr, G., Falkner, S., et al. 2017b, *A&A*, 597, A3  
Soffel, M., Herold, H., Ruder, H., & Ventura, J. 1985, *A&A*, 144, 485  
Sokolova-Lapa, E., Gornostaev, M., Wilms, J., et al. 2021, *A&A*, 651, A12  
Staubert, R., Trümper, J., Kendziorra, E., et al. 2019, *A&A*, 622, A61  
Tsygankov, S. S., Doroshenko, V., Poutanen, J., et al. 2022, *ApJ*, 941, L14  
van Adelsberg, M. & Lai, D. 2006, *MNRAS*, 373, 1495  
Ventura, J. 1979, *Phys. Rev. D*, 19, 1684  
Ventura, J., Nagel, W., & Meszaros, P. 1979, *ApJL*, 233, L125  
West, B. F., Wolfram, K. D., & Becker, P. A. 2017a, *ApJ*, 835, 129  
West, B. F., Wolfram, K. D., & Becker, P. A. 2017b, *ApJ*, 835, 130